LANGMUIR Article
Cite This: Langmuir 2017, 33, 11788-11796 pubs.acs.org/Langmuir

# Virial Coefficients and Equations of State for Hard Polyhedron Fluids

M. Eric Irrgang,[†] Michael Engel,[‡,§] Andrew J. Schultz,[∥] David A. Kofke,[∥] and Sharon C. Glotzer*[,†,‡]

[†]Department of Materials Science and Engineering, University of Michigan, Ann Arbor, Michigan 48109, United States
[‡]Department of Chemical Engineering, University of Michigan, Ann Arbor, Michigan 48109, United States
[§]Institute for Multiscale Simulation, Friedrich-Alexander-Universität Erlangen-Nürnberg, 91058 Erlangen, Germany
[∥]Department of Chemical and Biological Engineering, University at Buffalo, The State University of New York, Buffalo, New York 14260, United States

Supporting Information

**ABSTRACT:** Hard polyhedra are a natural extension of the hard sphere model for simple fluids, but there is no general scheme for predicting the effect of shape on thermodynamic properties, even in moderate-density fluids. Only the second virial coefficient is known analytically for general convex shapes, so higher-order equations of state have been elusive. Here we investigate high-precision state functions in the fluid phase of 14 representative polyhedra with different assembly behaviors. We discuss historic efforts in analytically approximating virial coefficients up to $B_4$ and numerically evaluating them to $B_8$. Using virial coefficients as inputs, we show the convergence properties for four equations of state for hard convex bodies. In particular, the exponential approximant of Barlow et al. (*J. Chem. Phys.* **2012**, *137*, 204102) is found to be useful up to the first ordering transition for most polyhedra. The convergence behavior we explore can guide choices in expending additional resources for improved estimates. Fluids of arbitrary hard convex bodies are too complicated to be described in a general way at high densities, so the high-precision state data we provide can serve as a reference for future work in calculating state data or as a basis for thermodynamic integration.

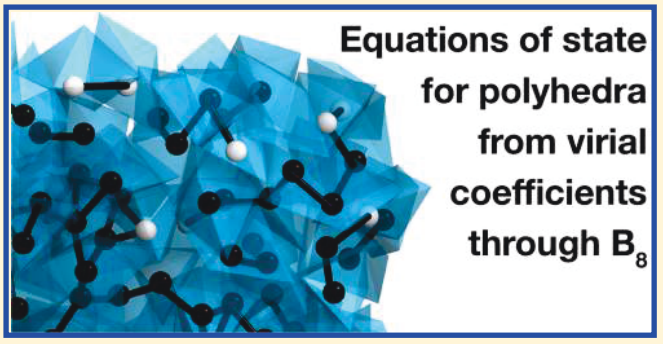


## INTRODUCTION

The thermodynamic behavior of molecules and colloidal particles is often dominated by shape,[2] but while the hard sphere (HS) system is a standard model for simple fluids, much less is known about nonspherical hard shapes. Padé approximant hard sphere equations of state (EOSs) have been studied for half a century,[3] and modern numerical techniques can calculate up to the 12th hard sphere virial coefficients with high precision.[4−6] In contrast, only the simplest of anisotropic shapes are described well analytically or in published numerical studies, and trends observed for specific families of shapes have not led to effective general expressions for even the third virial coefficient.[7]

Indeed, the difficulty in deriving an EOS for highly anisotropic polyhedra was discussed recently by Solana[8] with respect to the hard tetrahedron system for which high-precision virial coefficients are available.[9] Besides these tetrahedron data, we are not aware of other reports of virial coefficients for hard polyhedra.

Polyhedra are particularly interesting shapes because they are geometrically simple and can be synthesized with a high level of shape perfection and monodispersity in nanocrystals.[10] Simulation studies of hard polyhedra demonstrate a rich set of assembly phenomena greatly exceeding that of hard spheres.[11−13] The deviation from hard sphere behavior has been explained by the presence of well-defined facets, inducing local alignment.[14] As a result, the effective entropic interactions are directional, which affects the behavior of the hard polyhedron fluid even at intermediate densities. The knowledge of equations of state of hard polyhedra promises insights into the dynamics of hard polyhedron systems and is a prerequisite for the establishment of particle shape as a thermodynamic parameter.[15]

Here we study state functions of 14 hard polyhedra that were chosen to cover a range of asphericities and serve as representative for diverse assembly behavior. We determine the compressibility factors of the polyhedron fluids using Monte Carlo simulation and calculate the first eight virial coefficients by numerically evaluating cluster integrals. We discuss implications for historic semianalytic equations that incorporate geometric factors. Our findings test and compare the applicability and convergence of four forms of equations of state, each constructed in terms of arbitrary numbers of

**Special Issue:** Tribute to Keith Gubbins, Pioneer in the Theory of Liquids

**Received:** July 11, 2017
**Revised:** September 15, 2017
**Published:** September 15, 2017



  
DOI: 10.1021/acs.langmuir.7b02384
Langmuir 2017, 33, 11788−11796

available virial coefficients. We examine the virial expansion in density, a free volume expansion, a modification to an EOS described by Solana,[8] and the exponential approximant due to Barlow et al.[1] The functional forms of these equations are not capable of representing the sharp transition and coexistance region of a first-order phase transition, so we cannot expect to provide a single state function across multiple phases. Previous literature casts doubt[16] that convergence or divergence will be an effective way to predict phase transitions, but we are nevertheless surprised at the variety of behaviors observed across shapes, functional forms, and orders of error in EOS schemes.

We investigate 14 polyhedra, including three Platonic solids (tetrahedron, cube, and octahedron), three Archimedean solids (truncated tetrahedron, truncated cube, and truncated octahedron), a Catalan solid (rhombic dodecahedron), two Johnson solids (square pyramid and triangular dipyramid), and four additional polyhedra (triangular prism, pentagonal prism, hexagonal prism, and obtuse golden rhombohedron) with known phase behavior,[12] as well as the 90% truncated tetrahedron.[17]

## THEORY

The fluid EOS is commonly represented with dimensionless compressibility factor $Z$, which is the ratio of the fluid volume to that of an ideal gas at the same temperature $T$, pressure $p$, and number of particles $N$. For a simple fluid consisting of $N$ particles of uniform volume $v_0$, a convenient notation uses the reduced pressure $p^* = \beta p v_0$ with $\beta = (k_B T)^{-1}$ and the packing fraction $\eta = v_0\rho = v_0 N/V$ to write

$$Z = \frac{V}{V_{id}} = \frac{pV}{Nk_BT} = \frac{\beta p}{\rho} = \frac{p^*}{\eta} \tag{1}$$

The virial EOS is expressed as a power series in density to perturbatively describe the fluid phase relative to the ideal gas. The $j$th order virial EOS (VEOS$j$) is the power series

$$Z_{VEOSj} = 1 + \sum_{k=2}^{j} \hat{B}_k \rho^{k-1} = 1 + \sum_{k=2}^{j} B_k \eta^{k-1} \tag{2}$$

where $B_k = \hat{B}_k / v_0^{k-1}$ is the reduced $k$th virial coefficient.

The second virial coefficient captures the initial departure from ideal gas behavior and is the last coefficient that can be analytically solved for general hard convex bodies (HCBs). It is given by[18,19]

$$B_2 = 1 + \frac{RS}{v_0} = 1 + 3\alpha \tag{3}$$

where it is useful to define a size-independent shape asphericity $\alpha = RS/3v_0$ as a function of three fundamental shape measures: surface area $S$ of a single particle; $R$, the mean curvature integrated over the surface and normalized by $4\pi$; and particle volume $v_0$. $\alpha$ can be seen as relating the quantity $RS$ for a convex shape to that of a sphere of the same volume, such that $\alpha \equiv 1$ for a sphere.

It is possible to formulate equations of state that are parametrized using only $B_2$ but that are more accurate to higher densities than VEOS2 itself. Since van der Waals, it has been common to describe $Z$ not relative to the absolute volume, but to the non-excluded volume available to particles of finite size. Equation 4,[20] for example, is known[21] to converge faster than the VEOS for hard spheres. With $a_1 = 1$ and $a_2 = 3\alpha$, $Z_{FV2}$ is exact through $B_2$ but projects a better high-density fit for HCBs than VEOS2 does.

$$Z_{FVn}(\eta) = \sum_{m=1}^{n} a_m \frac{\eta^{m-1}}{(1-\eta)^m} \tag{4}$$

Values of $a_m$ can be calculated from known virial coefficients and tend to be of moderate magnitude.

A popular class of equations that extrapolates to higher density more accurately than a truncated virial expansion is the Padé approximant. Here, compressibility factor $Z$ is expressed as the ratio of two polynomials, the coefficients of which can be chosen by equating the first few terms of a Taylor expansion in $\eta$ to targeted virial coefficients. The best-known Padé approximant for hard spheres is the Carnahan–Starling (CS) equation,[3] which was proposed empirically and predicts $B_k = k^2 + k - 2$. More accurate approximants are possible within Percus–Yevick theory.[22] In this article, we will broadly define an approximant as any functional form that is constructed to capture the effect of higher-order terms in the density series, while adhering to the virial series to given order at low density.

Using $B_2$ and assuming $Z_0 = 1/(1-\eta)$ as the low-density limiting behavior,[a] Solana proposed[8] capturing the shape-dependent perturbations to the hard sphere EOS in a single term, $c(\eta)$. We note that deviation from $Z_{HS}$ is constrained to $B_3$ and higher if we first scale the sphere volume to match the known second virial coefficient. Using "effective hard sphere" $Z_{EHS}$, then, we have

$$Z_{S'}^{HCB}(\eta) = \frac{1}{1-\eta} + c(\eta)\left[Z_{EHS}(\eta) - \frac{1}{1-\eta}\right] \tag{5}$$

where $Z_{EHS}(\eta) = Z_{HS}(\eta_{eff})$ and $\eta_{eff} = \eta(1 + 3\alpha)/4$.

For the purposes of this article, we neglect geometric arguments for approximating $c(\eta)$ and choose instead to solve for coefficients $c_i$ in $c(\eta) = \sum_{i=0}^{j-2} c_i \eta^i$ using numerically calculated virial coefficients to construct an approximant of $j$th order. $c_0$ is necessarily unity for HCBs, and $c_i$ depends on virial coefficients up to $B_{i+2}^{HS}$ and $B_{i+2}^{HCB}$.

The third virial coefficient, $B_3$, is analytic for some particle shapes of high symmetry, and $B_4$ is known for hard spheres; however, only $B_2$ is generally solvable, e.g., for polyhedra. At higher densities, theoretical treatments must account for higher-order particle correlations. Rigorous studies of hard sphere systems[23] illustrate the potential utility of methodologies commonly supporting analytic expressions for third- and fourth-order approximants.

HCB approximants frequently incorporate $\alpha$ and other asphericity terms,[24] which give some metric of a shape in relation to that of a quantifiably related sphere. Equations are easily normalized for particle size, but at least two quantities are necessary to capture the available shape information in $R$, $S$, and $v_0$. In addition to $\alpha$, several equations of state[7,8,25] use a complementary geometric parameter ($\tau = 4\pi R^2/S$) that relates the surface area of a shape to that of a sphere with the same integrated mean curvature.[b]

Attempts at analytic expressions for $B_3$ frequently lead to expressions[27,28] of the form

$$B_3 = 1 + 6\alpha + G \tag{6}$$

with the limiting constraint that $G \to 3$ for spheres. Boublík originally asserted $G \approx 3\alpha^2$, while more recent works[7,25] explore its dependence on an independent shape parameter $\tau$. Kihara and Boublik reason that $G = 3\alpha^2\xi$ and attempt to



DOI: 10.1021/acs.langmuir.7b02384
Langmuir 2017, 33, 11788–11796

constrain $\xi$ to some simple form $\phi(\tau)$, such that $3\alpha^2\phi(\tau) = G = a_3$ in eq 4.

Solana's EOS yields $\boldsymbol{G} = 3\alpha + 3\frac{\partial c}{\partial \eta}\Big|_{\eta=0}$ with the implied constraints that, in the low-density limit $\eta \to 0^+$, $c(\eta) \to \alpha$ while the derivative $\frac{\partial}{\partial \eta}c$ goes to zero for spheres and is non-zero for nonspheres.

Gibbons presented a generalized EOS[29] that was later improved.[30,31] A variant by Song and Mason[32] (SM) projects to higher order by explicitly perturbing the hard sphere fourth virial coefficient.

Various proposed expressions for $B_4$ take the form $B_4 = 1 + 9\alpha + 3G + H$ but do not attempt to or succeed at describing polyhedra. We note, though, that $H$ is equivalent to $a_4$ from eq 4, and

$$\begin{aligned} B_4 &= a_1 + 3a_2 + 3a_3 + a_4 \\ &= 1 + 9\alpha + 3\boldsymbol{G} + a_4 \end{aligned} \tag{7}$$

Today, the computational cost of numerically determining $B_3$ and $B_4$ to high precision trivially surpasses the effectiveness of prior approximate methods. With knowledge of many numerically calculated virial coefficients, approximants can be constructed to arbitrary order.

Recently, Barlow et al.[1] introduced a generalized Padé approximant for repulsive spheres of arbitrary softness, which extrapolates from a chosen number of virial coefficients used as inputs. The effectiveness of the approximant is enhanced over conventional Padé approximants by enforcing the same high-density asymptotic behavior as the model fluid being described. In the hard sphere limit, the $j$th-order exponential approximant (EA$j$) takes the form of an exponential of a polynomial in density

$$Z_{\mathrm{EA}j} = \exp(N_2\eta + N_3\eta^2 + \ldots + N_j\eta^{j-1}) \tag{8}$$

with coefficients $N_i$ determined by matching the Taylor expansion of $Z_{\mathrm{EA}j}$ to known virial coefficients.

## METHODS

**Calculation of the Second Virial Coefficient.** We calculate the second virial coefficient analytically using the conventional HCB expression, eq 3, and three fundamental geometric measures.

Mean curvature (or the average of two principal curvatures) is most easily understood for a polyhedron as the limiting case of a spheropolyhedron as the rounding radius goes to zero. When the surface of a polyhedron is extended outward by a radius $r$, the facets, edges, and vertices become facets, cylindrical sections, and spherical sections, respectively, on the resulting spheropolyhedron. For the spherical sections, principle curvatures are $\kappa_1 = \kappa_2 = 1/r$, so mean curvature $H = {}^1/_2(\kappa_1 + \kappa_2) = 1/r$. On the cylindrical sections, one of the principal curvatures is zero, and $H = {}^1/_2r$. Mean curvature is zero on the facets.

Together, the spherical sections at the vertices comprise exactly one complete spherical surface, while the cylindrical sections along the edges have length $l_i$ and $\pi - \theta_i$ radians, where $\theta_i$ is the dihedral angle. Integrating the mean curvature over the surface of the spheropolyhedron is then straightforward

$$\begin{aligned} \int_\sigma H\ \mathrm{d}S &= \sum_{\text{facets}} \int 0\ \mathrm{d}S + \sum_{\text{vertices}} \int \frac{1}{r}\ \mathrm{d}S + \sum_{\text{edges}} \int \frac{1}{2r}\ \mathrm{d}S \\ &= \iint_{\text{sphere}} \frac{1}{r}r^2 \sin\theta\ \mathrm{d}\theta\ \mathrm{d}\phi + \sum_i \int_0^{l_i}\int_0^{\pi-\theta_i} \frac{1}{2r}r\ \mathrm{d}l\ \mathrm{d}\theta \\ &= 4\pi r + \sum_i l_i\frac{\pi - \theta_i}{2} \end{aligned} \tag{9}$$

In the limit as $r \to 0$, the (normalized) integrated mean curvature for a polyhedron is then given by

$$R = \frac{1}{4\pi}\int_\sigma H\ \mathrm{d}S = \frac{1}{4\pi}\sum_i l_i\frac{\pi - \theta_i}{2} \tag{10}$$

The summation runs over all edges with edge length $l_i$ and dihedral angle $\theta_i$ between adjacent faces.

The remaining fundamental measures in eq 3 are easy to calculate for convex polyhedra. The surface area due to the (triangulated) facets is given by the half-magnitude of the cross products of the edges, and the contributing volume of each is given by the volumes of the cones that share an apex at some interior point (such as the particle center of mass).

**Calculation of Higher Virial Coefficients.** Virial coefficients from $B_3$ to $B_8$ (eq 2) for all of the polyhedra studied are calculated numerically, following methods very similar to those recently used to compute virial coefficients of hard spheres.[5] We briefly review these methods here.

Each coefficient $B_k$ is given via the configurational integral (taking particle 1 to define the origin)

$$B_k = v_0^{1-k}\left(\frac{1-k}{k!}\right)\int f_{\mathrm{B}}(\mathbf{r}^k, \boldsymbol{\omega}^k)\ \mathrm{d}\mathbf{r}_2 \ldots \mathrm{d}\mathbf{r}_k\ \mathrm{d}\boldsymbol{\omega}_1 \ldots\ \mathrm{d}\boldsymbol{\omega}_k \tag{11}$$

with the orientation integrals normalized to unity: $\int \mathrm{d}\boldsymbol{\omega}_i = 1$. The integrand $f_{\mathrm{B}}$ is the sum of biconnected graphs[4]

$$f_{\mathrm{B}}(\mathbf{r}^k, \boldsymbol{\omega}^k) = \sum_G \left(\prod_{ij\in G} f_{ij}\right) \tag{12}$$

Graphs $G$ are formed from $k$ vertices, one for each particle appearing in the integral, with Mayer $f$-bonds joining some of the vertex pairs. For hard polyhedra, the Mayer function $f_{ij}$ for the particles labeled $i$ and $j$ in the configuration $(\mathbf{r}^k,\boldsymbol{\omega}^k)$ will be zero if they are not overlapping, and $-1$ otherwise. The product in eq 12 is taken over all pairs having a bond in graph $G$, and the sum is over all doubly connected graphs of $k$ vertices.

For each shape, we directly sample the full set of graphs efficiently by building up candidate configurations under simpler constraints.[5] Chains and trees are graphs having no closed loops and are easily generated randomly to form a template. Each bond in the template is satisfied by finding a random orientation and position for each sequentially placed polyhedron that overlaps the polyhedron at the neighboring vertex. Additional overlaps, occurring by chance, add bonds to the template to form the configuration graph.

The configuration graph is used for an initial screening to quickly identify some of those configurations for which $f_{\mathrm{B}}$ equals zero (for instance, we confirm that the configuration graph of polyhedra is doubly connected). If the configuration does not pass the screening, zero is added to the average. If it does pass, then we compute the integrand $f_{\mathrm{B}}(\mathbf{r}^k,\boldsymbol{\omega}^k)$ using Wheatley's recursive algorithm,[4] and we compute the sampling weight for the configuration, $\pi(\mathbf{r}^k,\boldsymbol{\omega}^k)$, using the methods detailed previously.[5] Virial coefficient $B_k$ is then given in terms of the average for this process, according to

$$B_k = v_0^{1-k}\left(\frac{1-k}{k!}\right)\left\langle\frac{f_{\mathrm{B}}}{\pi}\right\rangle_\pi \tag{13}$$

where the angle brackets indicate the computed average.

For the 14 representative polyhedra, we sample $1.45 \times 10^{11}$ configurations for each coefficient. Within this total, independent



DOI: 10.1021/acs.langmuir.7b02384
Langmuir 2017, 33, 11788−11796

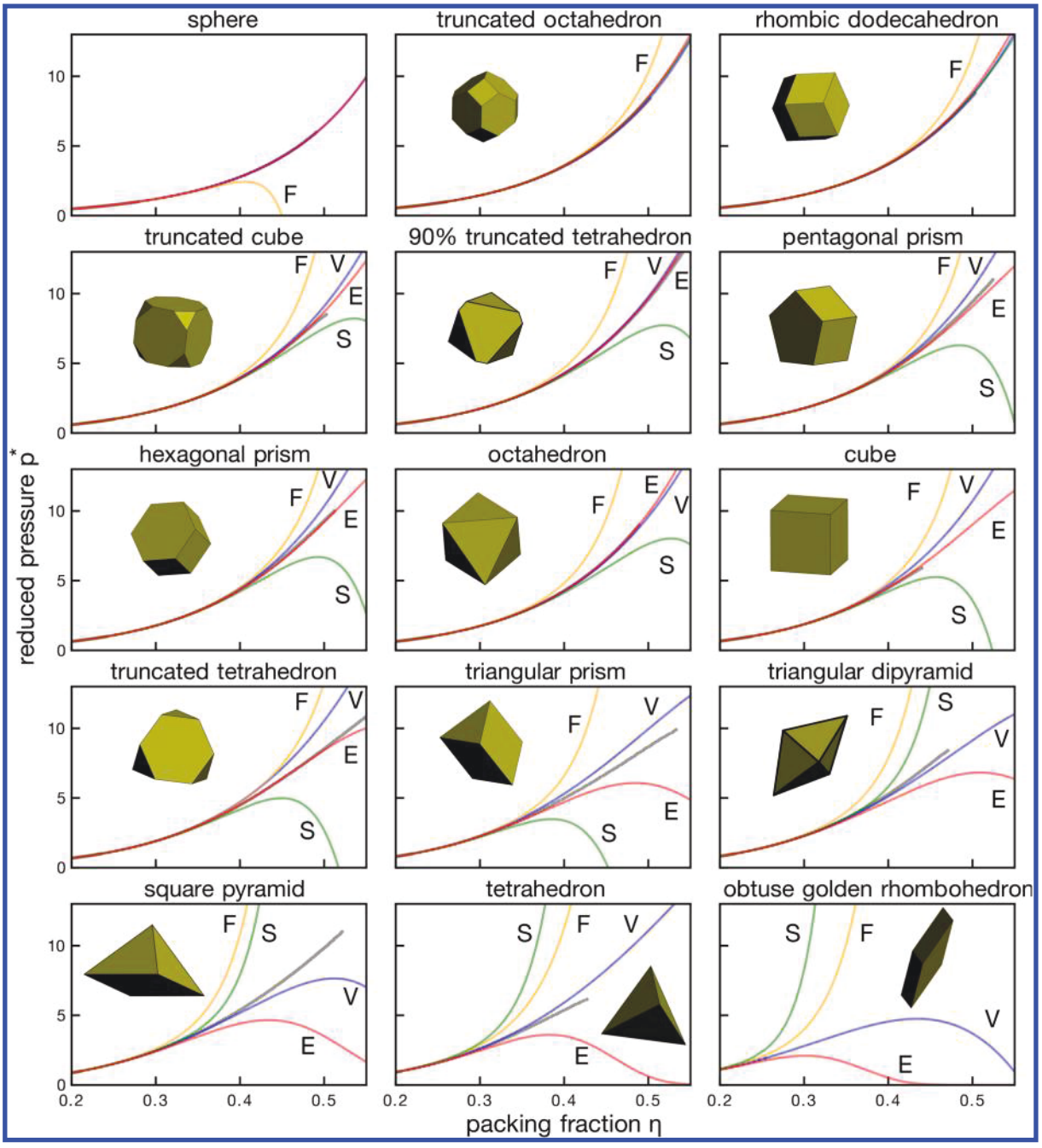


**Figure 1.** Pressure vs packing fraction for the sphere and 14 polyhedra. The subfigures are in order of increasing asphericity $\alpha$ from left to right and top to bottom. We compare the Monte Carlo simulation data (gray circular markers) with the four eighth-order approximants: the virial equation (eq 2) in blue, labeled "V"; the free volume EOS (eq 4) in orange, labeled "F"; the modified Solana EOS (eq 5) in green, labeled "S"; and the exponential approximant (eq 8) in red, labeled "E". The estimated error is not shown here but is more clearly illustrated in Figure 2 and in the Supporting Information. The Solana equation is meaningless for the hard sphere and is omitted from that subfigure.

sub-averages of $1 \times 10^8$ to $2 \times 10^9$ (varying with coefficient) samples are collected to generate uncertainty estimates, which are reported as one standard deviation of the mean (68% confidence level).

**Thermodynamic Monte Carlo Simulation of Hard Polyhedron Fluids.** We perform isobaric (constant-pressure) hard particle Monte Carlo simulations using standard methods employed previously.[12,33] At state points from $p^* = 10^{-4}$ to the freezing transition, we simulate each system with periodic boundary conditions and measure the packing fraction. Each simulation begins with $N = 2048$ particles positioned and oriented randomly at a moderate density, and we define a MC step to mean $N$ Monte Carlo trials. We initially targeted a relative uncertainty in packing fraction of $\leq 10^{-4}$ at up to 300 state points per shape, conservatively estimating a need to sample each state point up to 20 times with simulation trajectories up to $2.5 \times 10^6$ MC steps. In many cases, we have determined the sufficiency of fewer data for a state point and choose not to complete this protocol.

The hard sphere system fluid equilibrates easily within $0.5 \times 10^6$ MC steps even at high densities and within $0.1 \times 10^6$ steps at densities below $\eta \approx 0.25$. When $\eta \approx 0.25$, we observe that simulation densities for shaped particles converge by the time the Monte Carlo move sizes are optimized and fixed, variously at $0.2 \times 10^6$, $0.3 \times 10^6$, or $0.5 \times 10^6$ MC steps depending on the shape. For higher densities, then, the polyhedra are allowed to equilibrate for $1.5 \times 10^6$ MC steps, and then the packing fraction is measured over an additional $1.0 \times 10^6$ steps.



DOI: 10.1021/acs.langmuir.7b02384
Langmuir 2017, 33, 11788−11796

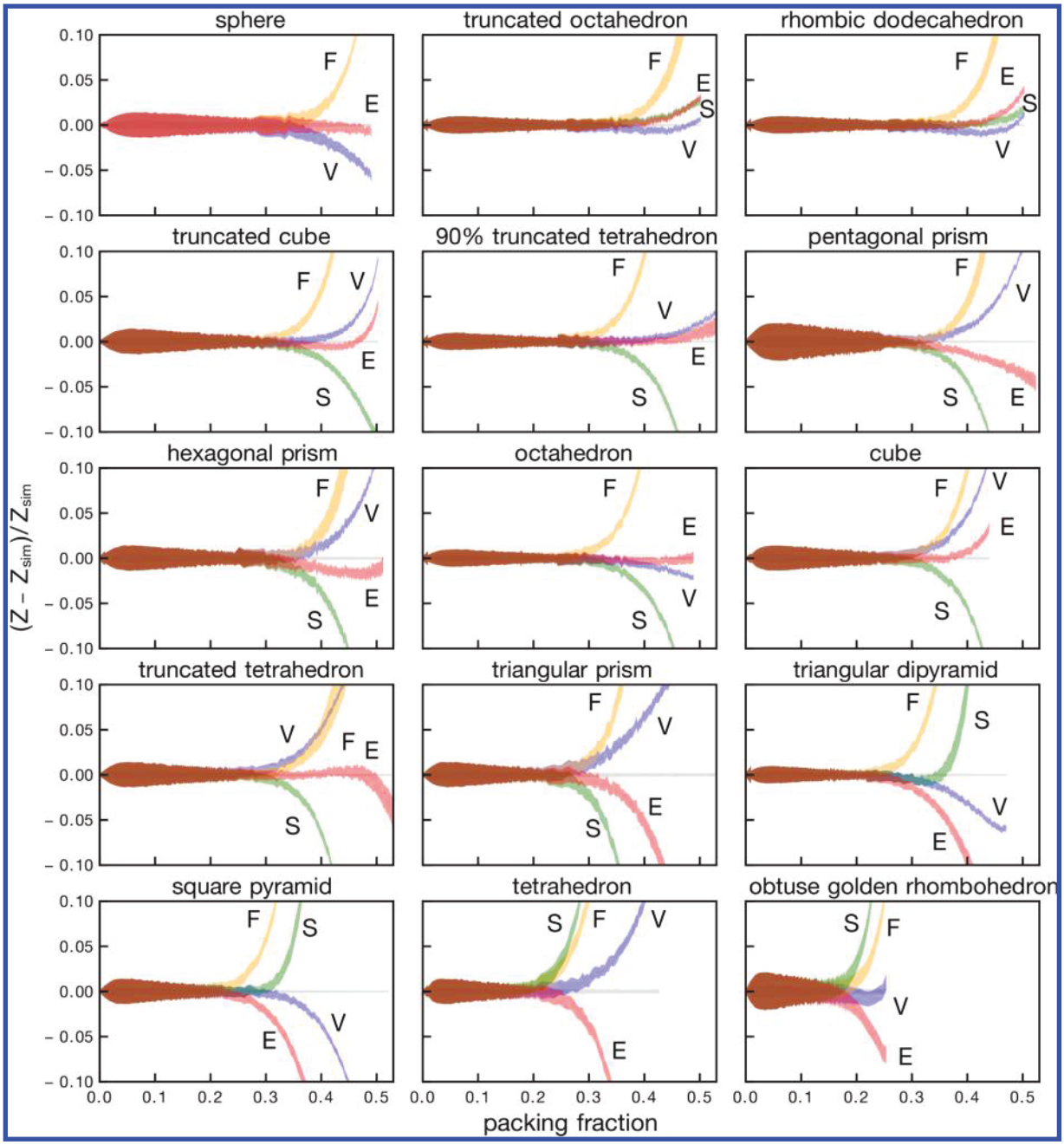


**Figure 2.** Deviations of the state functions from the simulation data for the sphere and 14 polyhedra. We show the relative difference for virial equation $Z_{VEOS8}$ (blue, "V", eq 2), free volume EOS $Z_{FV8}$ (orange, "F", eq 4), modified Solana EOS $Z_{Solana8}$ (green, "S", eq 5), and exponential approximant $Z_{EA8}$ (red, "E", eq 8), each normalized to the simulation data (gray). The estimated uncertainty in the vertical axis is represented by the $1\sigma$ filled regions. The width of the horizontal gray line reflects the estimated simulation uncertainty. The width of the EOS plot traces includes the uncertainty propagated from simulation due to the normalization, dominating other sources of error at low densities.

Below $\eta \approx 0.25$, the packing fraction is measured from the step at which MC parameters are fixed. To give equal weight, the value contributed to a packing fraction measurement is extracted from the same range of MC steps in each trajectory. Because, at lower packing fractions, we are able to achieve our desired precision before completing $2.5 \times 10^6$ MC steps, some computations were terminated early and the trajectories were truncated to $1.2 \times 10^6$ MC steps.

Because of fairly long correlations in the denser systems (see the Supporting Information), we do not expect a single trajectory to reasonably sample the entire ensemble and instead rely on independent simulations for uncorrelated measurements. Uncertainty in the state data is estimated from the standard error of the mean packing fraction from 5 to 20 independent simulations equilibrated and run with different random number seeds.

**Construction of Approximants.** Approximants of the various forms discussed are constructed to exactly reproduce an arbitrary number of virial coefficients. The free volume equation of state (eq 4) can easily be represented in terms of the numerically calculated virial coefficients with

$$a_m = \sum_{k=1}^{m} (-1)^{k+m} \binom{m-1}{k-1} B_k \tag{14}$$

and uncertainty propagated by



DOI: 10.1021/acs.langmuir.7b02384
Langmuir 2017, 33, 11788−11796

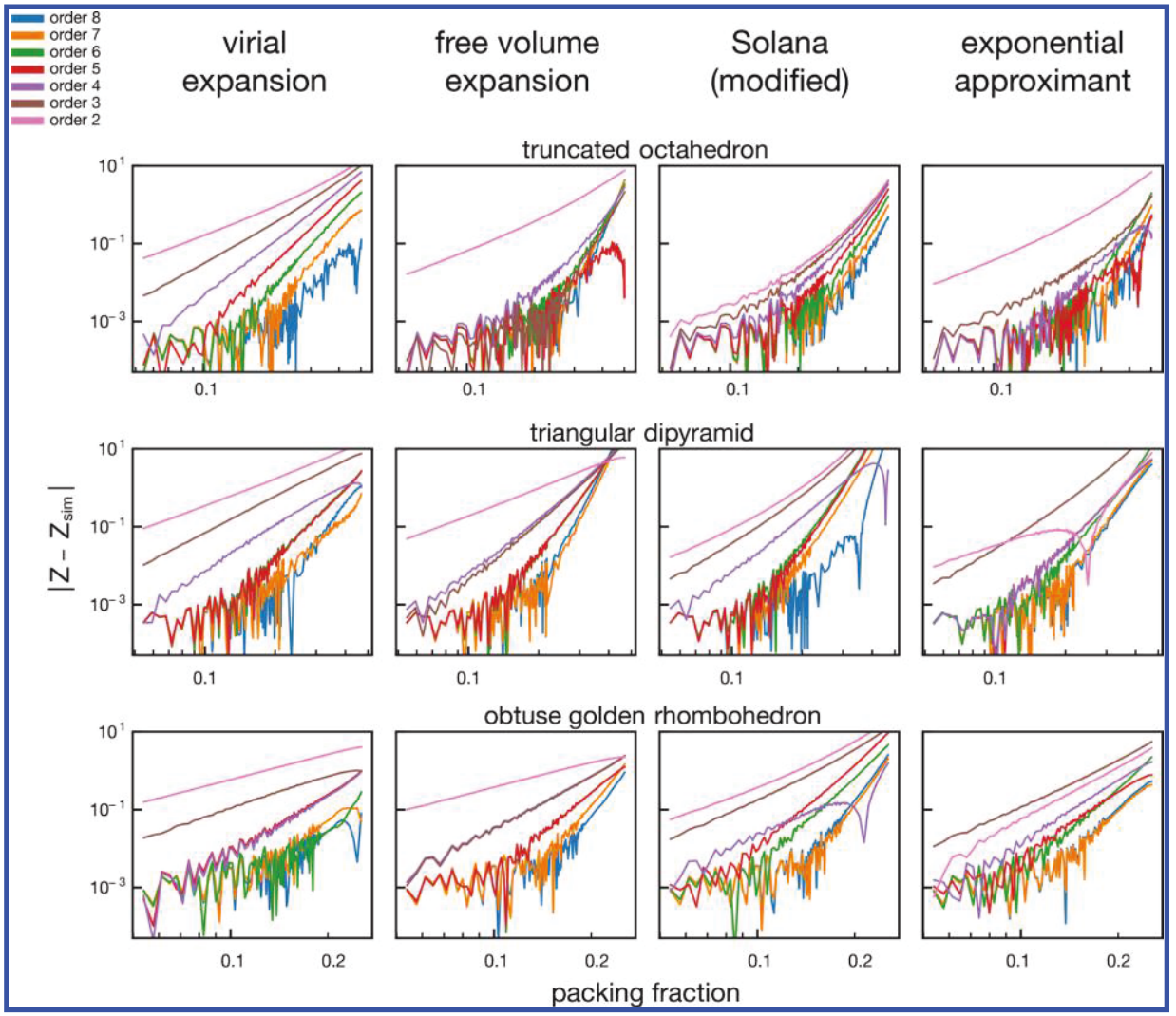


**Figure 3.** Convergence of the $j$th-order equations of state for selected shapes at $\alpha = 1.18$, $\alpha = 1.97$, and $\alpha = 2.85$. We show the absolute difference from NpT simulation data for virial equation $Z_{\mathrm{VEOS}j}$ (eq 2), free volume EOS $Z_{\mathrm{FV}j}$ (eq 4), modified Solana EOS $Z_{\mathrm{Solana}j}$ (eq 5), and exponential approximant $Z_{\mathrm{EA}j}$ (eq 8), plotted vs packing fraction. The log−log scale emphasizes the nature of the dominant error terms. For ease of visualization, error bars were omitted and data were connected by lines to aid the eye. Because the vertical axis shows an absolute value, apparent poles in some graphs occur after an EOS has begun to diverge in the opposite direction from its accumulated error, re-intersecting the simulation data. The horizontal axis scale is adjusted for each shape to allow maximal detail. Plots for the remaining shapes are included in the Supporting Information.

$$\sigma^2_{Z_{\mathrm{FV}j}} = \sum_{k=2}^{j}\left[\sum_{m=k}^{j}(-1)^{k+m}\binom{m-1}{k-1}\frac{\eta^{m-1}}{(1-\eta)^m}\sigma_{B_k}\right]^2 \quad (15)$$

The other approximants (eqs 5 and 8) are less trivial, but free parameters are solved by expressing a Taylor series expansion around $\eta = 0$ and equating terms to known reduced virial coefficients. This is easily performed by computer algebra (in this case with Wolfram Mathematica) along with the derived uncertainty propagated from the virial coefficients. For EOS orders 3−8, we have calculated $a_m$ (eq 4), $c_i$ (eq 5), and $N_k$ (eq 8).

## RESULTS AND DISCUSSION

We did not equilibrate simulations through the first ordering transition of each shape, and we do not claim to precisely locate the ordering transitions. In the cases of the hard sphere, octahedron, and triangular dipyramid, the apparently equilibrated fluid data extend to pressures in metastable regions, but in these cases, we restrict our comparisons to densities below the first ordering transitions noted in the literature.[34−36] The obtuse golden rhombohedron undergoes a liquid crystal transition above $\eta \approx 0.25$ or $p^* = 1.9$, so we restrict our EOS analysis to the disordered fluid.

Figures 1 and 2 compare semianalytic equations of state to our simulation data. Up to the triangular prism, the exponential approximant provides the best eighth-order EOS, generally staying within measurement precision longer and diverging later than the other EOSs. For more aspherical shapes, the eighth-order VEOS and modified Solana EOS are as good or better. Remarkably, the VEOS describes the obtuse golden rhombohedron within 1−2% up to the liquid crystal transition, while the approximants all diverge at somewhat lower densities.

For densities less than approximately half of the first ordering transition, compressibility values from the approximants generally converge quickly (Figure 3). All of the approximants match the simulation data better to higher densities than the VEOS at third order, and for low asphericity, all three outperform the VEOS as high as seventh order. At fourth order and higher, the exponential approximant generally remains within 1% and within 5% to higher densities than



DOI: 10.1021/acs.langmuir.7b02384
Langmuir 2017, 33, 11788−11796

Table 1. Higher Virial Coefficients of the Sphere and 14 Polyhedra[a]

| | shape | $B_3$ | $B_4$ | $B_5$ | $B_6$ | $B_7$ | $B_8$ |
|---|---|---|---|---|---|---|---|
| 1 | sphere[5] | 10 | 18.364768 | 28.2244(1) | 39.8151(9) | 53.341(2) | 68.54(1) |
| 2 | truncated octahedron | 12.84591(4) | 26.2284(2) | 43.672(1) | 64.387(6) | 85.87(4) | 102.4(3) |
| 3 | rhombic dodecahedron | 13.47750(4) | 27.8331(2) | 46.194(1) | 66.904(7) | 86.98(4) | 102.3(3) |
| 4 | truncated cube | 15.06275(4) | 32.0594(3) | 52.559(1) | 69.522(9) | 71.01(6) | 46.5(5) |
| 5 | 90% truncated tetrahedron | 16.74906(5) | 36.4986(3) | 58.887(2) | 72.34(1) | 62.93(9) | 31.2(8) |
| 6 | pentagonal prism | 17.01593(5) | 37.9864(3) | 64.318(2) | 85.53(1) | 80.73(10) | 23.4(8) |
| 7 | hexagonal prism | 17.01369(5) | 37.5649(3) | 62.642(2) | 82.87(1) | 81.63(10) | 38.2(8) |
| 8 | octahedron | 17.00537(5) | 36.9035(3) | 58.149(2) | 67.07(1) | 49.9(1) | 17.6(8) |
| 9 | cube | 18.30341(5) | 41.8485(4) | 70.709(2) | 88.33(2) | 63.5(1) | −37(1) |
| 10 | truncated tetrahedron | 19.19187(6) | 43.5694(4) | 70.297(3) | 79.02(2) | 41.4(2) | −67(1) |
| 11 | triangular prism | 25.24793(8) | 61.7590(6) | 94.874(5) | 60.08(4) | −136.0(4) | −526(4) |
| 12 | triangular dipyramid | 26.92203(8) | 62.4752(7) | 78.641(6) | 5.06(5) | −193.0(5) | −355(6) |
| 13 | square pyramid | 30.15558(9) | 74.2408(8) | 94.432(7) | −27.56(7) | −375.4(8) | −697(9) |
| 14 | tetrahedron | 33.0247(1) | 80.7475(10) | 85.029(9) | −90.60(9) | −325(1) | 200(10) |
| 15 | obtuse golden rhombohedron | 47.9196(2) | 117.349(2) | 13.20(2) | −676.2(3) | −1257(4) | 1910(60) |

[a] $B_k$ values are the dimensionless reduced virial coefficients, normalized by $v_0^{k-1}$ as in eq 2. Sphere virial coefficients are analytic to $B_4$. All other virial coefficients are determined numerically.

Table 2. Derived Free Volume Coefficients $a_k$ of the Sphere and 14 Polyhedra for eq 4[a]

| | shape | $a_2$ | $a_3$ | $a_4$ | $a_5$ | $a_6$ | $a_7$ | $a_8$ |
|---|---|---|---|---|---|---|---|---|
| 1 | sphere | 3.0 | 3.0 | −0.6352316 | −0.23462(10) | 1.34058(40) | −2.4782(23) | 3.180(14) |
| 2 | truncated octahedron | 3.5511711 | 4.743567(36) | 0.344145(91) | −1.37116(43) | 1.6094(23) | −3.564(14) | 3.984(87) |
| 3 | rhombic dodecahedron | 3.6742346 | 5.129036(38) | 0.42328(10) | −1.97068(49) | 1.8630(28) | −3.084(17) | 4.53(11) |
| 4 | truncated cube | 3.9644254 | 6.133901(43) | 0.76447(13) | −4.15968(68) | 0.5151(40) | −1.769(27) | 9.35(18) |
| 5 | 90% truncated tetrahedron | 4.2670168 | 7.215030(48) | 1.05248(17) | −6.68128(91) | 0.7410(59) | 2.821(41) | 10.56(30) |
| 6 | pentagonal prism | 4.2928988 | 7.430131(48) | 1.81730(17) | −5.70339(91) | −0.8914(60) | −2.926(42) | 11.55(31) |
| 7 | hexagonal prism | 4.3094011 | 7.394892(49) | 1.45205(17) | −5.77281(93) | 0.7160(62) | −2.899(44) | 8.19(32) |
| 8 | octahedron | 4.3189880 | 7.367391(49) | 0.84436(17) | −7.70900(96) | 0.9040(62) | 5.809(45) | 12.25(33) |
| 9 | cube | 4.5 | 8.303408(52) | 2.43827(20) | −7.8650(11) | −3.2600(75) | −0.268(55) | 16.48(42) |
| 10 | truncated tetrahedron | 4.6692106 | 8.853451(56) | 2.00141(22) | −10.5066(13) | −1.3440(92) | 5.172(70) | 3.45(55) |
| 11 | triangular prism | 5.5801270 | 13.087678(75) | 4.75562(38) | −25.9955(27) | −17.281(22) | 31.72(20) | 43.8(19) |
| 12 | triangular dipyramid | 5.9220598 | 14.077909(83) | 1.47527(45) | −36.4161(34) | 0.995(31) | 70.05(30) | 18.6(30) |
| 13 | square pyramid | 6.3040560 | 16.547463(92) | 4.68620(55) | −49.8136(44) | −23.344(42) | 131.14(42) | 62.3(45) |
| 14 | tetrahedron | 6.7037158 | 18.61728(10) | 3.78451(67) | −69.6277(57) | −1.000(58) | 329.22(62) | −222.1(69) |
| 15 | obtuse golden rhombohedron | 8.5595086 | 29.80059(16) | 1.2689(14) | −205.921(16) | −1.13(20) | 1313.4(28) | −785(40) |

[a] Values for $a_2$ are analytic for all shapes shown. Other coefficients are calculated by matching terms in the power series in $\eta$ to the numerically calculated virial coefficients.

the other EOS for shapes with asphericity $\alpha \lesssim 1.8$, but results are rather varied for higher asphericities.

Figure 3 illustrates the effectiveness of the approximants at projecting to higher order than the virial coefficients on which they are based. At low order, the free volume equation of state captures higher than $O(\eta^j)$ terms (apparent in the slope of the error) and is within measurement precision to >10% packing fraction. In fact, the third-order free volume EOS is superior to its fourth-order version as well as the other EOSs. The plots for the free volume EOS seem to show $|Z_{fv} - Z_{sim}|$ passing through the same point after emerging from the noise at successively higher densities, though the ordering of the plots from left to right does not in fact correspond to the increasing order of the EOS. If such a trend held, however, we would have the remarkable finding that an important density could be discerned simply by looking for zeroes in an expression of the difference between EOSs of successive order [e.g., $Z_{EOS(n+1)} - Z_{EOS(n)} = 0$]. Additional plots in the Supporting Information clarify that the trend is not particularly strong, nor is the indicated density precise. Nevertheless, we note that the free volume EOS is unique among the equations studied in appearing to very nearly mark the density of the liquid crystal transition.

We list coefficients for VEOS8 and FV8 in Tables 1 and 2. $B_3$, $B_4$, and $a_3$, as well as $\tau$ (Table 3), are all nearly monotonic in $\alpha$ for the polyhedra studied, but $a_4$, calculated from virial coefficients, appears to amplify whatever information is available at lower order and appears to be less strongly correlated to asphericity. The predictive power of geometric quantities is less clear for higher virial coefficients, which become large and negative for highly aspherical polyhedra. This behavior suggests that the Song−Mason EOS and other Padé approximants that depend on only low-order virial coefficients are unlikely to capture thermodynamic behavior for general hard convex bodies.

In several cases, we find that the magnitude of a virial coefficient decreases substantially from the previous term, only to increase in a subsequent term. Apparently oscillatory behavior in virial coefficients has been previously reported,[9] and our data support an assertion that the convergence of a



DOI: 10.1021/acs.langmuir.7b02384
Langmuir 2017, 33, 11788−11796

Table 3. Geometric Quantities $\alpha = (RS)/(3v_0)$, $\tau = 4\pi(R^2/S)$, and $B_2 = 1 + 3\alpha$[a]

| | shape | $\alpha$ | $\tau$ | $B_2$ |
|---|---|---|---|---|
| 1 | sphere | 1.0 | 1.0 | 4.0 |
| 2 | truncated octahedron | 1.183723696 | 1.055618663 | 4.551171089 |
| 3 | rhombic dodecahedron | 1.224744871 | 1.110720735 | 4.674234614 |
| 4 | truncated cube | 1.321475138 | 1.070529044 | 4.964425413 |
| 5 | 90% truncated tetrahedron | 1.422338938 | 1.422338938 | 5.267016815 |
| 6 | pentagonal prism | 1.430966283 | 1.139815072 | 5.292898848 |
| 7 | hexagonal prism | 1.436467026 | 1.122382953 | 5.309401077 |
| 8 | octahedron | 1.439662680 | 1.253110832 | 5.318988041 |
| 9 | cube | 1.5 | 1.178097245 | 5.5 |
| 10 | truncated tetrahedron | 1.556403524 | 1.129390052 | 5.669210573 |
| 11 | triangular prism | 1.860042340 | 1.269711916 | 6.580127019 |
| 12 | triangular dipyramid | 1.974019921 | 1.396134539 | 6.922059762 |
| 13 | square pyramid | 2.101351984 | 1.360539523 | 7.304055953 |
| 14 | tetrahedron | 2.234571934 | 1.509477606 | 7.703715802 |
| 15 | obtuse golden rhombohedron | 2.853169549 | 1.317152762 | 9.559508647 |

[a]Values calculated exactly to nine decimal places with Mathematica except for the 90% truncated tetrahedron (a nonstandard shape), calculated with 64-bit numerical precision using 9-digit vertex coordinates.

virial series cannot be concluded from the appearance of a single small coefficient.

Remarkably, $\alpha$ appears to effectively sort shapes by the onset and magnitude of these oscillations. Virial coefficients of the most spherical shapes appear to be monotonically increasing, but the trend is broken at lower order and to a greater degree in direct correspondence to increasing $\alpha$. Negative virial coefficients appear with the cube ($\alpha = 1.5$), occurring at lower order and/or greater magnitude with each asphericity sampled.

While $\tau$ clearly contains information different from that of $\alpha$, its utility in thermodynamic prediction is not evident in this study. We note, however, that expressions involving $\tau$ tend to appear in contexts including shapes much more aspherical than ours.

The breakdowns of the approximants for the triangular prism, the triangular dipyramid, the square pyramid, and the tetrahedron coincide with sign changes and large magnitudes of higher-order virial coefficients. All approximants fail beyond the first ordering transition, which can be crystallization or the formation of a liquid crystal (e.g., the nematic phase at $\eta = 0.25$ for the obtuse golden rhombohedron), but also fail to predict the phase change. No clear pattern emerges as to which EOSs become clearly nonphysical before the phase change, while others continue to describe the metastable fluid to higher densities. As expected, none of the equations studied are accurate beyond the isotropic fluid phase.

## CONCLUSION

We have computed high-precision state data and virial coefficients for pure fluids of 14 relevant polyhedra to compare several power series and approximant equations of state. The virial EOS and the exponential approximant have coefficients solved with Monte Carlo solutions to the configurational cluster integrals. The free volume EOS coefficients and the coefficients in our modification of Solana's EOS are calculated in terms of the mapping to virial coefficients. We evaluate the virial EOS, a free volume EOS, a modification to an EOS based on hard spheres (due to Solana), and an exponential approximant due to Barlow et al. to consider which equations make the best use of numerically evaluated cluster integrals for orders 3−8.

Each of the four equations may be expressed as an expansion in density to arbitrary order, and though we are unable to make strong statements regarding convergence in these expansions, the free volume expansion in particular has a tantalizing tendency to imply divergence at some density near the first ordering transition. A rigorous determination of the first ordering transition densities may provide better background for further investigation.

More insight may be possible with additional virial coefficients, but because computing higher-order cluster integrals quickly becomes astronomically expensive, some scheme of extrapolating to higher order is likely necessary. The graphical information in Figure 3 is available for all shapes in the Supporting Information, along with the simulation state data for further numerical analysis.

When no numerically approximated virial coefficients are available, polyhedra with asphericity less than $\alpha \approx 1.8$ are best represented by their "effective sphere", equivalent to the trivial case of setting $c(\eta) \equiv 1$ in eq 5.

We show that the free volume EOS (eq 4) can be a particularly convenient and effective tool for estimation or for reducing the computational cost of hard particle studies. Given the equation's simplicity and the ease with which $B_3$ can be calculated numerically, the equation can provide an excellent starting point for thermodynamic integration. If a researcher wants to integrate the pressure−volume state function in the fluid regime, eq 4 provides at least three or four digits of precision up to densities of ≥10%, requiring particle simulations to be run at only moderate and higher densities.

If more virial coefficients are available, the exponential approximant provides a good alternative to the virial EOS, particularly for shapes less aspherical than $\alpha = 1.6$ to $\alpha = 1.8$; the maximum density to which each equation is accurate for a given $\alpha$ depends on the required precision. Additional data are provided in the Supporting Information for thermodynamic reference data or to guide expenditure of computational effort in constructing an approximant for a chosen purpose.

## ASSOCIATED CONTENT

### Supporting Information

The Supporting Information is available free of charge on the ACS Publications website at DOI: 10.1021/acs.langmuir.7b02384.

Additional visualization of data and descriptions of methods (PDF)

State data for each simulated shape in columns of pressure, packing fraction, and standard error of the mean packing fraction (ZIP)

## AUTHOR INFORMATION


### Corresponding Author

*E-mail: sglotzer@umich.edu.

### ORCID

David A. Kofke: 0000-0002-2530-8816

Sharon C. Glotzer: 0000-0002-7197-0085




DOI: 10.1021/acs.langmuir.7b02384
Langmuir 2017, 33, 11788−11796

### Notes

The authors declare no competing financial interest.

## ■ ACKNOWLEDGMENTS

The authors gratefully acknowledge discussions with Rolfe Petschek, Amir Haji-Akbari, Greg van Anders, and Pablo Damasceno. M.E.I., M.E., and S.C.G. acknowledge support by the DOD/ASD(R&E) under Grant N00244-09-1-0062 for concept development and initial implementation and by the National Science Foundation, Division of Materials Research Award DMR 1409620, for calculation of the EOS data for all of the studied polyhedron fluids. A.J.S. and D.A.K. acknowledge support by the National Science Foundation, Division of Chemistry Grant CHE 1464581. M.E. acknowledges funding by Deutsche Forschungsgemeinschaft through the Cluster of Excellence Engineering of Advanced Materials (EXC 315/2). Computational resources and services were supported by Advanced Research Computing at the University of Michigan and by the University at Buffalo Center for Computational Research.

## ■ ADDITIONAL NOTES

[a]In fact, $Z_0 = 1/(1 - 4\eta)$ for hard spheres, or $Z_0 = 1/[1 - (1 + 3\alpha)\eta]$ for general HCBs, would give exact behavior to $B_2$ but is obviously unsuitable as the basis for an extrapolation to a higher density due to the pole.

[b]$\tau$ and other simple asphericity metrics are neither clearly orthogonal to $\alpha$ nor as well motivated as quantities of thermodynamic relevance. With the knowledge that $R$, $S$, and $v_0$ are all easily mapped to the set of Minkowski tensors,[26] it may be that higher-order information on a shape function could help in understanding HCB thermodynamic behavior, but the authors cannot offer any insight at this time.

## ■ REFERENCES

(1) Barlow, N. S.; Schultz, A. J.; Weinstein, S. J.; Kofke, D. A. An asymptotically consistent approximant method with application to soft- and hard-sphere fluids. *J. Chem. Phys.* **2012**, *137*, 204102.
(2) Glotzer, S. C.; Solomon, M. J. Anisotropy of building blocks and their assembly into complex structures. *Nat. Mater.* **2007**, *6*, 557−62.
(3) Carnahan, N. F.; Starling, K. E. Equation of State for Nonattracting Rigid Spheres. *J. Chem. Phys.* **1969**, *51*, 635.
(4) Wheatley, R. J. Calculation of high-order virial coefficients with applications to hard and soft spheres. *Phys. Rev. Lett.* **2013**, *110*, 200601.
(5) Schultz, A. J.; Kofke, D. A. Fifth to eleventh virial coefficients of hard spheres. *Phys. Rev. E* **2014**, *90*, 23301.
(6) Zhang, C.; Pettitt, B. M. Computation of high-order virial coefficients in high-dimensional hard-sphere fluids by Mayer sampling. *Mol. Phys.* **2014**, *112*, 1427−1447.
(7) Boublík, T. Third and fourth virial coefficients and the equation of state of hard prolate spherocylinders. *J. Phys. Chem. B* **2004**, *108*, 7424−7429.
(8) Solana, J. Equations of state of hard-body fluids: a new proposal. *Mol. Phys.* **2015**, *113*, 1003−1013.
(9) Kolafa, J.; Labík, S. Virial coefficients and the equation of state of the hard tetrahedron fluid. *Mol. Phys.* **2015**, *113*, 1119.
(10) Xia, Y.; Xiong, Y.; Lim, B.; Skrabalak, S. E. Shape-Controlled Synthesis of Metal Nanocrystals: Simple Chemistry Meets Complex Physics? *Angew. Chem., Int. Ed.* **2009**, *48*, 60−103.
(11) Agarwal, U.; Escobedo, F. A. Mesophase behaviour of polyhedral particles. *Nat. Mater.* **2011**, *10*, 230−235.
(12) Damasceno, P. F.; Engel, M.; Glotzer, S. C. Predictive Self-Assembly of Polyhedra into Complex Structures. *Science* **2012**, *337*, 453−457.
(13) Gantapara, A. P.; De Graaf, J.; van Roij, R. R. R.; Dijkstra, M. Phase Diagram and Structural Diversity of a Family of Truncated Cubes: Degenerate Close-Packed Structures and Vacancy-Rich States. *Phys. Rev. Lett.* **2013**, *111*, 015501.
(14) van Anders, G.; Klotsa, D.; Ahmed, N. K.; Engel, M.; Glotzer, S. C. Understanding shape entropy through local dense packing. *Proc. Natl. Acad. Sci. U. S. A.* **2014**, *111*, E4812−E4821.
(15) van Anders, G.; Klotsa, D.; Karas, A. S.; Dodd, P. M.; Glotzer, S. C. Digital Alchemy for Materials Design: Colloids and Beyond. *ACS Nano* **2015**, *9*, 9542−9553.
(16) Schultz, A. J.; Kofke, D. A. Vapor-phase metastability and condensation via the virial equation of state with extrapolated coefficients. *Fluid Phase Equilib.* **2016**, *409*, 12−18.
(17) Damasceno, P. F.; Engel, M.; Glotzer, S. C. Crystalline assemblies and densest packings of a family of truncated tetrahedra and the role of directional entropic forces. *ACS Nano* **2012**, *6*, 609−614.
(18) Isihara, A. Determination of Molecular Shape by Osmotic Measurement. *J. Chem. Phys.* **1950**, *18*, 1446.
(19) Hadwiger, H. Der kinetische Radius nichtkugelförmiger Moleküle. *Experientia* **1951**, *7*, 395−398.
(20) Kolafa, J.; Labík, S.; Malijevský, A. Accurate equation of state of the hard sphere fluid in stable and metastable regions. *Phys. Chem. Chem. Phys.* **2004**, *6*, 2335.
(21) Mulero, A.; Galán, C.; Cuadros, F. Equations of state for hard spheres. A review of accuracy and applications. *Phys. Chem. Chem. Phys.* **2001**, *3*, 4991−4999.
(22) Santos, A. Chemical-Potential Route: A Hidden Percus-Yevick Equation of State for Hard Spheres. *Phys. Rev. Lett.* **2012**, *109*, 120601.
(23) Müller, E. A.; Gubbins, K. E. Triplet correlation function for hard sphere systems. *Mol. Phys.* **1993**, *80*, 91−101.
(24) Boublík, T.; Nezbeda, I. P-V-T behaviour of hard body fluids. Theory and experiment. *Collect. Czech. Chem. Commun.* **1986**, *51*, 2301−2432.
(25) Naumann, K. H.; Leland, T. W. Conformal solution methods based on the hard convex body expansion theory. *Fluid Phase Equilib.* **1984**, *18*, 1−45.
(26) Schröder-Turk, G. E.; Mickel, W.; Kapfer, S. C.; Schaller, F. M.; Breidenbach, B.; Hug, D.; Mecke, K. Minkowski tensors of anisotropic spatial structure. *New J. Phys.* **2013**, *15*, 083028.
(27) Boublík, T. Hard convex body equation of state. *J. Chem. Phys.* **1975**, *63*, 4084.
(28) Kihara, T.; Miyoshi, K. Geometry of three convex bodies applicable to three-molecule clusters in polyatomic gases. *J. Stat. Phys.* **1975**, *13*, 337−345.
(29) Gibbons, R. M. The scaled particle theory for particles of arbitrary shape. *Mol. Phys.* **1969**, *17*, 81−86.
(30) Nezbeda, I. Virial expansion and an improved equation of state for the hard convex molecule system. *Chem. Phys. Lett.* **1976**, *41*, 55−58.
(31) Boublík, T. Equations of state of hard body fluids. *Mol. Phys.* **1986**, *59*, 371−380.
(32) Song, Y.; Mason, E. A. Equation of state for a fluid of hard convex bodies in any number of dimensions. *Phys. Rev. A: At., Mol., Opt. Phys.* **1990**, *41*, 3121−3124.
(33) Haji-Akbari, A.; Engel, M.; Keys, A. S.; Zheng, X.; Petschek, R. G.; Palffy-Muhoray, P.; Glotzer, S. C. Disordered, quasicrystalline and crystalline phases of densely packed tetrahedra. *Nature* **2009**, *462*, 773−777.
(34) Fernández, L. A.; Martín-Mayor, V.; Seoane, B.; Verrocchio, P. Equilibrium Fluid-Solid Coexistence of Hard Spheres. *Phys. Rev. Lett.* **2012**, *108*, 165701.
(35) Ni, R.; Gantapara, A. P.; de Graaf, J.; van Roij, R.; Dijkstra, M. Phase diagram of colloidal hard superballs: from cubes via spheres to octahedra. *Soft Matter* **2012**, *8*, 8826.
(36) Haji-Akbari, A.; Engel, M.; Glotzer, S. C. Degenerate Quasicrystal of Hard Triangular Bipyramids. *Phys. Rev. Lett.* **2011**, *107*, 215702.



DOI: 10.1021/acs.langmuir.7b02384
*Langmuir* 2017, 33, 11788−11796